"ice" may be to some extent coincidental. It is possible that material in the deep interior contains both a component which is lighter than "ice," perhaps hydrogen and helium, and one which is heavier, that is, rock, and is more or less uniformly mixed. Fixing the interior rock/"ice" ratio to the solar value, we find for Uranus and Neptune that the total mass fraction of free hydrogen and helium is about 0.14 in both planets, with about one-third to one-fifth of this component (that is, about 0.05 in N1 and N3, and about 0.03 in N2) in the outermost atmospheric region at pressures smaller than 100 kbar, and the remainder distributed uniformly through the interior.

With such a small total mass fraction of hydrogen and helium, the deuterium to hydrogen number ratio (D/H) in the atmospheres of Uranus and Neptune should be about the same, and equal to the elevated value for primordial ices in other water-rich solar system bodies, that is, about 2×10^{-4}, rather than equal to the primordial nebular value of about 2×10^{-5} which is seen in the atmospheres of Jupiter and Saturn (*21*). Recent observations of deuterium in the atmospheres of Uranus and Neptune have confirmed that this is the case (*22*).

One of the most striking differences between Uranus and Neptune is the substantial net interior heat flow for Neptune. The heat flow for Uranus is so far undetectable and significantly smaller than the value for Neptune (*23*). Attempts to model this difference have taken the path of either relating it to differences in interior structure, with the possibility of pronounced chemical gradients suppressing heat flow in Uranus (*24*), or to relating it to atmospheric effects which may suppress convection in Uranus due to its greater proximity to the sun (*17, 25, 26*). The similarity of interior structure which we infer here, and which had been suggested in earlier models (*27*), makes the second explanation more attractive.

REFERENCES AND NOTES

1. B. A. Smith *et al.*, *Science* **246**, 1422 (1989).
2. G. L. Tyler *et al.*, *ibid.*, p. 1466.
3. J. W. Warwick *et al.*, *ibid.*, p. 1498.
4. W. M. Owen, Jr., R. M. Vaughn, S. P. Synnott, *Astron. J.* **101**, 1511 (1991).
5. A. C. Mitchell and W. J. Nellis, *J. Chem. Phys.* **76**, 6273 (1982).
6. W. J. Nellis *et al.*, *Science* **240**, 779 (1988).
7. H. B. Radousky, A. C. Mitchell, W. J. Nellis, *J. Chem. Phys.* **93**, 8235 (1990).
8. V. N. Zharkov and V. P. Trubitsyn, *Physics of Planetary Interiors* (Pachart, Tucson, AZ, 1978); W. B. Hubbard, *Planetary Interiors* (Van Nostrand Reinhold, New York, 1984).
9. S. S. Limaye, L. A. Sromovsky, V. E. Suomi, *Adv. Space Res.*, in press.
10. S. S. Limaye and L. A. Sromovsky, *J. Geophys. Res.*, in press.
11. V. E. Suomi, S. S. Limaye, D. R. Johnson, *Science* **251**, 929 (1991).
12. W. B. Hubbard, *Icarus* **52**, 509 (1982).
13. J.-L. Tassoul, *Theory of Rotating Stars* (Princeton Univ. Press, Princeton, NJ, 1978), p. 167.
14. W. B. Hubbard and M. S. Marley, *Icarus* **78**, 102 (1989).
15. D. Gautier and T. Owen, in *Origin and Evolution of Planetary and Satellite Atmospheres*, S. K. Atreya, J. B. Pollack, M. S. Matthews, Eds. (Univ. of Arizona Press, Tucson, 1989), pp. 487–512.
16. M. Ross, in *High Pressure in Research and Industry*, C. M. Backman, T. Johannisson, L. Tegner, Eds. (Arkitektkopia, Uppsala, 1982), vol. 2, pp. 721–727.
17. M. Podolak, R. T. Reynolds, R. Young, *Geophys. Res. Lett.* **17**, 1737 (1990).
18. R. G. Prinn and B. Fegley, *Astrophys. J.* **249**, 308 (1981).
19. R. G. French *et al.*, *Icarus* **73**, 349 (1988).
20. W. B. Hubbard *et al.*, *Nature* **319**, 636 (1986).
21. W. B. Hubbard and J. J. MacFarlane, *Icarus* **44**, 676 (1980).
22. C. de Bergh, B. L. Lutz, T. Owen, J.-P. Maillard, *Astrophys. J.* **355**, 661 (1990).
23. J. C. Pearl *et al.*, *Icarus* **84**, 12 (1990).
24. M. Podolak, W. B. Hubbard, D. J. Stevenson, in *Uranus*, J. T. Bergstrahl, E. D. Miner, M. S. Matthews, Eds. (Univ. of Arizona Press, Tucson, in press).
25. W. B. Hubbard and J. J. MacFarlane, *J. Geophys. Res.* **85**, 225 (1980).
26. A. P. Ingersoll and C. C. Porco, *Icarus* **35**, 27 (1978).
27. M. Podolak, R. Young, R. T. Reynolds, *ibid.* **63**, 266 (1985).

28. Work at the University of Arizona was supported by NASA grant NAGW-1555. Work at Lawrence Livermore National Laboratory was performed under the auspices of the U.S. Department of Energy under contract W-7405-ENG-48, with partial support from NASA under contract W-16.180. The "synthetic Uranus" was provided by M. Nicol of UCLA.

1 May 1991; accepted 5 July 1991

Relations Among Fault Behavior, Subsurface Geology, and Three-Dimensional Velocity Models

ANDREW J. MICHAEL AND DONNA EBERHART-PHILLIPS

The development of three-dimensional P-wave velocity models for the regions surrounding five large earthquakes in California has lead to the recognition of relations among fault behavior and the material properties of the rocks that contact the fault at seismogenic depths; regions of high moment release appear to correlate with high seismic velocities whereas rupture initiation or termination may be associated with lower seismic velocities. These relations point toward a physical understanding of why faults are divided into segments that can fail independently, an understanding that could improve our ability to predict earthquakes and strong ground motion.

FAULTS EXHIBIT BEHAVIORS RANGING from aseismic creep to brittle rupture in great earthquakes. Along the length of one fault, these variations can divide the fault into segments that fail independently (*1*). To investigate the mechanism controlling these variations, we have determined three-dimensional (3-D) P-wave velocity (V_P) models for the regions surrounding five moderate-to-large earthquakes in California. The 3-D V_P models, derived from local earthquake arrival-time data, provide indications of variations in the subsurface geology at seismogenic depths that may relate to the slip behavior of the faults. The five mainshocks studied (Fig. 1) are the magnitude M = 6 1966 Parkfield earthquake, the M = 6.7 1983 Coalinga earthquake (*2*), the M = 6.1 1985 Kettleman Hills earthquake (*2*), the M = 6.2 1984 Morgan Hill earthquake (*3*), and the M = 7.1 1989 Loma Prieta earthquake (*4*).

We calculated the 3-D V_P models using simultaneous inversion of local arrival-time data for the velocity model and the locations of the seismic sources. The arrival time of a seismic wave at a seismographic station depends on the time at which the wave originated (origin time), the location from which the wave originated (hypocenter), the location of the station, and the seismic velocities of the rocks along the raypath from the source to the station. The hypocenter, and sometimes the origin time, are known for explosions, whereas neither is known for earthquakes. The inversion process starts with initial estimates of the velocity model,

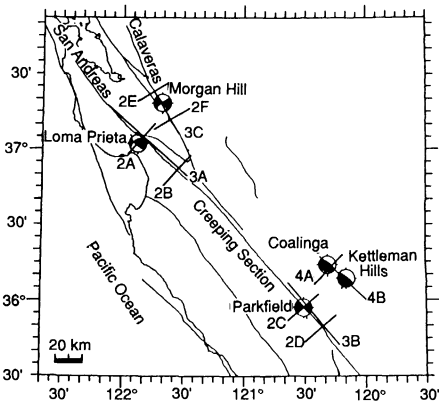

Fig. 1. Map of the five mainshocks studied showing their focal mechanisms, the locations of the cross sections shown in Figs. 2, 3, and 4 and the San Andreas and Calaveras faults.

Branch of Seismology, Mail Stop 977, U.S. Geological Survey, 345 Middlefield Road, Menlo Park, CA 94025.

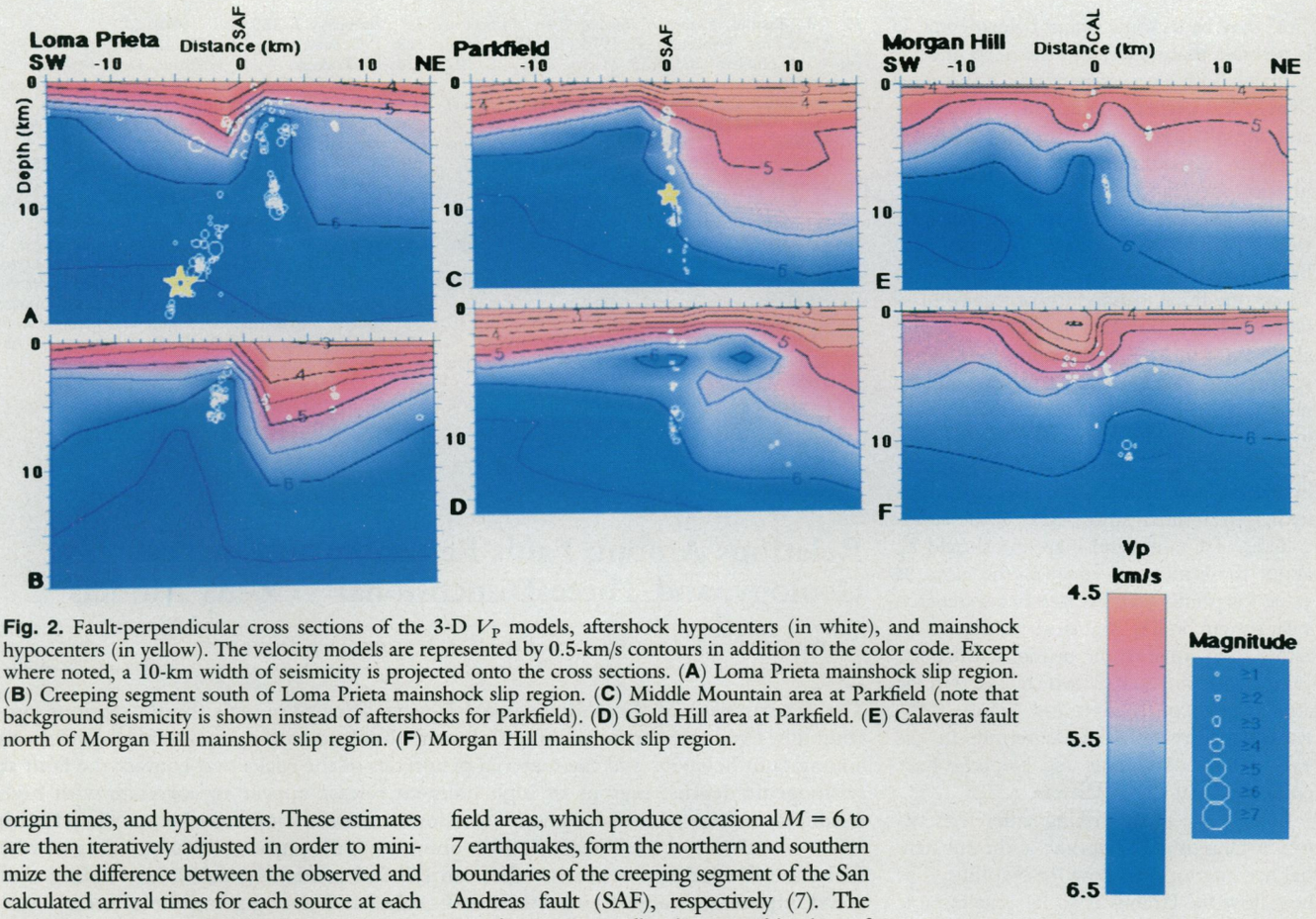

Fig. 2. Fault-perpendicular cross sections of the 3-D V_P models, aftershock hypocenters (in white), and mainshock hypocenters (in yellow). The velocity models are represented by 0.5-km/s contours in addition to the color code. Except where noted, a 10-km width of seismicity is projected onto the cross sections. (**A**) Loma Prieta mainshock slip region. (**B**) Creeping segment south of Loma Prieta mainshock slip region. (**C**) Middle Mountain area at Parkfield (note that background seismicity is shown instead of aftershocks for Parkfield). (**D**) Gold Hill area at Parkfield. (**E**) Calaveras fault north of Morgan Hill mainshock slip region. (**F**) Morgan Hill mainshock slip region.

origin times, and hypocenters. These estimates are then iteratively adjusted in order to minimize the difference between the observed and calculated arrival times for each source at each station.

In the particular method we used (*5*), the velocity model is parameterized at an irregularly spaced grid of nodes, and velocity is linearly interpolated between nodes. In our models, the node spacing is a minimum of 2 km; thus, the velocity changes appear as gradients rather than discrete discontinuities. An approximate 3-D ray-tracing technique (*6*) was used to calculate realistic ray paths and accurate arrival times in highly heterogeneous media.

Each of the four V_P models discussed below is based on several thousand arrival times from a few hundred earthquakes and up to 26 explosions recorded by stations of the U.S. Geological Survey Central California seismic network and a variety of temporary networks. The sources and stations are within, or close to, the area being modeled; maximum separations are 80 km. For each area, a preliminary inversion was performed with a coarse grid of roughly 80 by 100 km. Then, more detailed models were calculated, which extend 60 to 100 km along fault strike, 20 to 30 km across fault, and to 16 km in depth. The resolution is greatest where both the number and variety of ray paths are greatest, which is the seismogenic part of the fault.

The 3-D V_P models image the structure in four areas of the Pacific–North American plate boundary (Fig. 1). The Loma Prieta and Parkfield areas, which produce occasional $M = 6$ to 7 earthquakes, form the northern and southern boundaries of the creeping segment of the San Andreas fault (SAF), respectively (*7*). The creeping segment slips in a combination of aseismic creep events and frequent earthquakes of $M < 5$. The Morgan Hill area is part of the Calaveras fault, a strike-slip fault that has a long-term slip rate approximately 50% less than that of the SAF (*8*). In the Coalinga and Kettleman Hills area, young folds are underlain by blind thrust faults that rupture in moderate earthquakes (*9*).

In the creeping section of the SAF (*10*), the velocity model images the fault as a simple, sharp, horizontal V_P gradient (*11*) (Fig. 2, B and C). Where the Loma Prieta and Parkfield mainshocks produced the most slip, the SAF has more complicated velocity images. The cross section through the rupture zone of the Loma Prieta earthquake shows higher V_P on the southwest side at depths below 10 km, but higher V_P on the northeast side above that depth (Fig. 2A). Where most of the slip in the 1966 Parkfield mainshock took place (*12*), the V_P structure (Fig. 2D) surrounding the SAF is complicated and includes small bodies of high-velocity material. These relations suggest that the fault creeps where it is a well-developed structure that has, over the seismogenic depth interval, either a uniform contrast in material properties across the fault or a low V_P material on at least one side. Where the velocity structure near the fault zone is more complicated, the slip behavior tends to be brittle failure in larger events. At Morgan Hill the mainshock segment does not adjoin a creeping segment but rather terminates against a segment that has only $M < 5.5$ events and source dimensions of less than 10 km (*13*). In this northern segment, the fault is well imaged in the velocity model (Fig. 2E). In the section that ruptured during the $M = 6.2$ mainshock, the Calaveras fault is harder to define (Fig. 2F), and the behavior may thus be similar to that observed at Parkfield and Loma Prieta.

At Loma Prieta (Fig. 3A) the along-fault extent of material with $V_P > 6$ km/s at depths of less than 7 km coincides with the area that is inferred to have ruptured during the mainshock (*14*). At Parkfield (Fig. 3B) the mainshock initiated under the low V_P volume at Middle Mountain (*15*), but most of the moment release occurred adjacent to the high V_P material centered under Gold Hill. This material is in contact with the fault for a length similar to the maximum slip area determined for the 1966 mainshock (*12*). At Morgan Hill, the mainshock also initiated under a body of low V_P material; then the rupture propagated along the fault to an along-strike section that has more material with $V_P > 5.5$ km/s in contact with the fault. Most of the moment was released in this section (*16*) (Fig 3C).

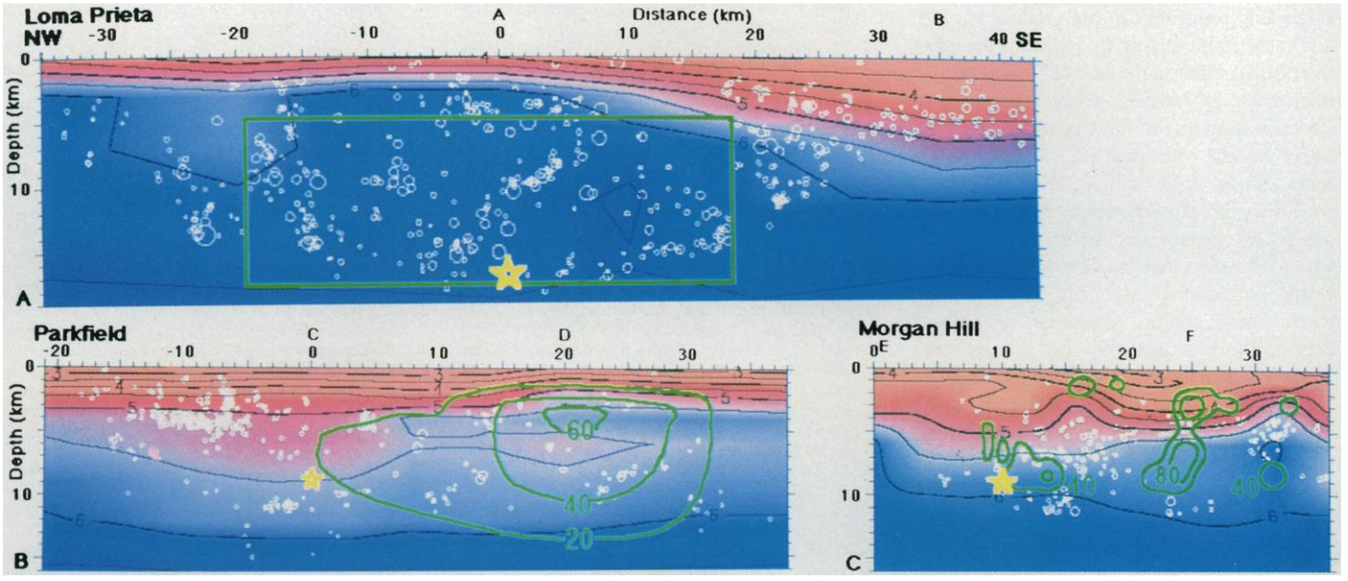

Fig. 3. Along-fault cross sections of the 3-D velocity models, aftershock hypocenters (in white), mainshock hypocenters (in yellow), and mainshock slip distributions (in green). We show the side of the fault that has the greater along strike V_P variations in the area surrounding the mainshock rupture; the other side of the fault is shown at selected points in Fig. 2. The letters above the cross sections show the locations of the cross sections in Fig. 2, A to F. (**A**) Northeast side of San Andreas fault in Loma Prieta region. Green rectangle is boundary of uniform slip region from geodetic modeling (*14*). A 15-km width of seismicity is projected onto this cross section. (**B**) Northeast side of San Andreas fault in Parkfield region (note that background seismicity is shown instead of aftershocks for Parkfield). Green contours (from 20 cm to 60 cm) show mainshock slip from geodetic modeling (*12*). (**C**) Southwest side of Calaveras fault in Morgan Hill region. Green contours (from 40 cm to 80 cm) show mainshock slip from seismic waveform modeling (*16*).

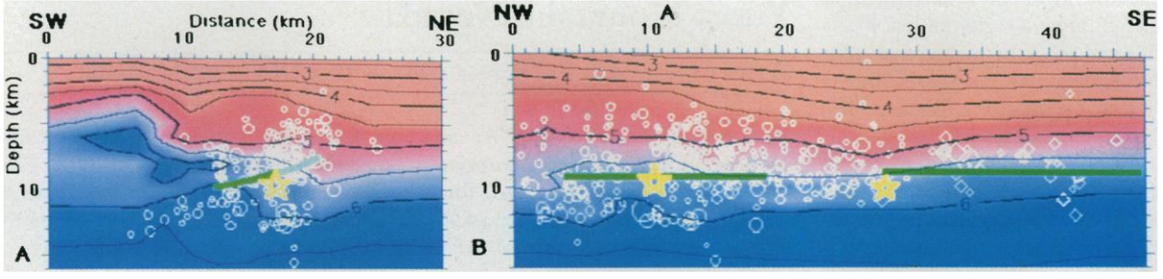

Fig. 4. Cross sections of the 3-D velocity model for the Coalinga–Kettleman Hills region, aftershock hypocenters (in white, circles: Coalinga, diamonds: Kettleman Hills), mainshock hypocenters (in yellow), and location of mainshock and postseismic slip determined from geodetic modeling (*17*) (in green). (**A**) Cross section across Coalinga anticline. The dark green curve shows the extent of coseismic slip and the light green curve shows the postseismic slip. (**B**) Along-anticline cross section. The green lines show the along-strike extent of coseismic slip.

The V_P model for Coalinga shows that the above relations between spatial variations in V_P and rupture mode may also apply to thrust faults. The Coalinga , mainshock ruptured through rocks of the Franciscan sequence that have $5.7 < V_P < 6.2$ km/s; the upward termination of the rupture is near the contour V_P = 5.7 km/s, which is the inferred boundary between the Franciscan and Great Valley sequence rocks (*2*) (Fig. 4A). Above this boundary the rupture continued, but in an aseismic mode during the following 4 years (*17*). Thus, the updip extent of the mainshock rupture area is associated with variations in the material properties that surround the fault.

Like mainshocks, microseismicity patterns may also be related to the variations in the velocity models. At Parkfield (Figs. 2C and 3B) the densest clusters of background seismicity are associated with the sharp across-fault V_P contrast where uniformly low V_P material contacts the northeast side of the SAF. The same is true of the background seismicity at Loma Prieta. Viewed along the anticline axis, the Coalinga and Kettleman Hills aftershocks are generally confined to rocks that have V_P of 4.5 to 6.0 km/s (Fig. 4B). Both of these V_P contours vary in depth along the anticline, along with the seismicity. At Morgan Hill, few earthquakes occur within a low V_P sedimentary basin (*3*) (Figs. 2, E and F, and 3C). These observations imply that the boundaries of the seismogenic zone are related to the variable material properties.

We have shown that within California (*18*) there may be a general relation between increasing V_P and increasing ability of the rocks to store strain energy and release it as brittle failure. A notable limitation on this relation is that the seismogenic zone in California extends to only about 15-km depth. Below this depth, increasing V_P does not indicate greater tendency toward brittle failure because of the effect of higher temperatures on the rheology (*19*).

The relation between V_P and the mode of

strain release can be explained in two ways. High fluid pressures can both reduce V_P (*20*) and cause stable sliding by reducing the effective normal stress on the fault (*21*). This process is probable at Parkfield where a few lines of evidence suggest the fluid pressures are high under Middle Mountain (*22*). If the low V_P rocks exhibit stable sliding, then the locked zone may be smaller where such rocks are present to greater depths; in this case the amount of strain that can be stored in that area would be reduced (*23*). Thus in those areas where stable sliding is present to unusual depths, the fault may not be able to store enough strain to produce large earthquakes. This notion could account for the limits on the rupture of the Loma Prieta earthquake and why little moment was released near the hypocenters of the Morgan Hill and Parkfield earthquakes.

Another possibility is that the areas with high displacement in the geodetic and seismic-waveform models actually represent areas where the stress drop is high and that the true slip pattern covers a wider area. This scenario is possible because in these models a uniform rigidity is used to convert the observed stress drop to slip. Thus a larger area may slip during the mainshock, but the geodetic and waveform observations are primarily sensitive to the areas of the fault that have a high rigidity and high V_P (*24*). In either case a dynamic rupture might end when it attempts to propagate through a region of low V_P.

If the material properties of the fault zone and the surrounding rocks control the manner in which the fault produces earthquakes, then V_P models could be used in earthquake prediction. For instance, current long-term prediction methods rely on our ability to identify fault segments that will fail in individual large earthquakes (*25*). Identification of fault segments has been based on surface geology, historic seismicity, and microseismicity (*13, 25, 26*); however, such observations are not always available or definitive. The use of V_P models to augment these techniques may help to identify segment boundaries. Proper fault segmentation and identification of the parts of a fault segment likely to release the most moment could also allow improved prediction of strong ground motions.

REFERENCES AND NOTES

1. C. R. Allen, *Stanford Univ. Publ. Geol. Sci.* **11**, 70 (1968).
2. D. Eberhart-Phillips, *J. Geophys. Res.* **94**, 15,565 (1989); *ibid.* **95**, 15,343 (1990).
3. A. J. Michael, *Bull. Seismol. Soc. Am.* **78**, 1199 (1988).
4. D. Eberhart-Phillips, V. F. Labson, W. D. Stanley, A. J. Michael, B. D. Rodriguez, *Geophys. Res. Lett.* **17**, 1235 (1990).
5. C. H. Thurber, thesis, Massachusetts Institute of Technology (1988).
6. J. Um and C. H. Thurber, *Bull. Seismol. Soc. Am.* **77**, 972 (1987).
7. W. H. Bakun and T. V. McEvilly, *J. Geophys. Res.* **89**, 3051 (1984); W. H. Bakun and A. G. Lindh, *Science* **229**, 619 (1985); U.S. Geological Survey Staff, *ibid.* **247**, 286 (1990).
8. M. Matsu'ura, D. D. Jackson, A. Cheng, *J. Geophys. Res.* **91**, 12,661 (1984); W. H. Prescott, M. Lisowski, J. C. Savage, *ibid.* **86**, 10,853 (1981).
9. C. M. Wentworth and M. D. Zoback, *Tectonics* **8**, 237 (1989).
10. The 3-D velocity models determined for the Loma Prieta and Parkfield regions by other workers show good resemblance to our models where the regions studied overlap; this similarity demonstrates that the 3-D inversions of V_P are a stable process. For example, A. Michelini, W. Foxall, T. V. McEvilly, *Seismol. Res. Lett.* **61**, 48 (1990); A. Michelini and T. V. McEvilly, *Bull. Seismol. Soc. Am.* **81**, 524 (1991).
11. With 2-D and 3-D V_P models, respectively, R. L. Wesson [*Bull. Seismol. Soc. Am.* **61**, 729 (1971)] and C. H. Thurber (*5*) also found a sharp velocity discontinuity across the creeping section of the San Andreas fault.
12. P. Segall and R. Harris, *J. Geophys. Res.* **92**, 10,511 (1987). We plot the model shown in their figure 8B.
13. D. H. Oppenheimer, W. H. Bakun, A. G. Lindh, *ibid.* **95**, 8483 (1990).
14. M. Lisowski, W. H. Prescott, J. C. Savage, M. J. Johnston, *Geophys. Res. Lett.* **17**, 1437 (1990).
15. C. M. Poley, A. G. Lindh, W. H. Bakun, and S. S. Schulz [*Nature* **327**, 134 (1987)] showed that the Middle Mountain area had larger-than-usual strain response to the remote stress change from the Coalinga earthquake. This response might have been anticipated on the basis of the implied low rigidity and shear modulus of the low V_P material underlying Middle Mountain.
16. S. H. Hartzell and T. H. Heaton, *Bull. Seismol. Soc. Am.* **76**, 649 (1986).
17. G. Ekstrom, R. S. Stein, J. P. Eaton, D. Eberhart-Phillips, *J. Geophys. Res.*, in press; R. S. Stein and G. Ekstrom, in preparation.
18. J. R. Grasso [*Geophys. Res. Lett.* **10**, 229 (1983)] proposed that a high-velocity barrier marked the termination of an $M = 5.1$ event in the Pyrenees. As this is the size of some Loma Prieta aftershocks, this observation may agree with ours.
19. R. H. Sibson, *Bull. Seismol. Soc. Am.* **72**, 151 (1982).
20. M. R. J. Wyllie, A. R. Gregory, G. H. F. Gardner, *Geophysics* **23**, 459 (1958); T. Todd and G. Simmons, *J. Geophys. Res.* **77**, 3731 (1972); N. I. Christensen, *Geophys. J. R. Astron. Soc.* **79**, 411 (1984); D. Eberhart-Philips, D. Han, M. D. Zoback, *Geophysics* **82**, 82 (1989).
21. J. H. Dieterich, *Pure Appl. Geophys.* **116**, 790 (1978).
22. The material under Middle Mountain has low velocities and low resistivity, but normal gravity; these data suggest that the low velocities are caused by high pore pressures. This notion is also supported by the high V_P/V_S in this area (*10*). The spatial association of potentially high pore pressures with aseismic creep was suggested by W. P. Irwin and I. Barnes, *Geology* **3**, 713 (1975).
23. C. H. Scholz, *Bull. Seismol. Soc. Am.* **72**, 1 (1982).
24. J. C. Jaeger and N. G. W. Cook, *Fundamentals of Rock Mechanics* (Chapman and Hall, London, ed. 3, 1979), p. 354.
25. Working Group on California Earthquake Probabilities, *U.S. Geol. Surv. Open-File Rep. 88-398* (1988); D. P. Schwartz and R. H. Sibson, Eds., *ibid. 89-315* (1989).
26. G. King and J. Nabelek, *Science* **228**, 984 (1985).

27. We thank M. Blanpied, S. Hickman, D. Hill, A. Lindh, D. Oppenheimer, and two anonymous reviewers for thoughtful reviews of this manuscript.

4 February 1991; accepted 20 May 1991

$^{40}Ar/^{39}Ar$ Age of the Lathrop Wells Volcanic Center, Yucca Mountain, Nevada

BRENT D. TURRIN, DUANE CHAMPION, ROBERT J. FLECK

Paleomagnetic and $^{40}Ar/^{39}Ar$ analyses from the Lathrop Wells volcanic center, Nevada, indicate that two eruptive events have occurred there. The ages (136 ± 8 and 141 ± 9 thousand years ago) for these two events are analytically indistinguishable. The small angular difference (4.7°) between the paleomagnetic directions from these two events suggests they differ in age by only about 100 years. These ages are consistent with the chronology of the surficial geological units in the Yucca Mountain area. These results contradict earlier interpretations of the cinder-cone geomorphology and soil-profile data that suggest that at least five temporally discrete eruptive events occurred at Lathrop Wells approximately 20,000 years ago.

THE SOUTHWEST PART OF THE NEVADA Test Site (NTS) is being evaluated to determine its suitability for a high-level radioactive waste repository (*1–4*). Study of the chronology and eruptive volumes of lava from nearby volcanos are essential for assessing volcanic hazards during the mandated 10^4-year isolation period for the high-level radioactive waste.

Within the NTS, silicic volcanic activity produced several coalesced caldera complexes during the Miocene (14 to 8 million years ago) (*5, 6*). Since then, volcanism has been limited to small, isolated subalkaline to alkaline undersaturated basaltic volcanic centers (*7, 8*). The most recent volcanic activity at the NTS occurred at the Lathrop Wells volcanic center. A recent geomorphic and soil profile study suggested that at least five temporally discrete eruptive events occurred at Lathrop Wells at approximately 20 ka (thousand years ago) (*9*); these studies have large chronologic uncertainties and contradict radiometric and paleomagnetic data (*10*). We dated seven sites (Table 1) using the $^{40}Ar/^{39}Ar$ method to further evaluate the isotopic age of the Lathrop Wells volcanic center.

At the Lathrop Wells volcanic center,

B. D. Turrin, U.S. Geological Survey, 345 Middlefield Road, Menlo Park, CA 94025, and Institute of Human Origins, Geochronology Center, 2453 Ridge Road, Berkeley, CA 94709.
D. Champion and R. J. Fleck, U.S. Geological Survey, 345 Middlefield Road, Menlo Park, CA 94025.